Chapter 4

Solution-Processed Graphene-Based Transparent Conductive Electrodes as Ideal ITO Alternatives for Organic Solar Cells

Minas M. Stylianakis, Dimitrios Konios,
Konstantinos Petridis and Emmanuel Kymakis

Additional information is available at the end of the chapter

http://dx.doi.org/10.5772/67919

Abstract

The isolation of free-standing graphene in 2004 was the spark for a new scientific revolution in the field of optoelectronics. Due to its extraordinary optoelectronic and mechanical properties, graphene is the next wonder material that could act as an ideal low-cost alternative material for the effective replacement of the expensive conventional materials used in organic optoelectronic applications. Indeed, the enhanced electrical conductivity of graphene combined with its high transparency in visible and near-infrared spectra, enabled graphene to be an ideal low-cost indium tin oxide (ITO) alternative in organic solar cells (OSCs). The prospects and future research trend in graphene-based TCE are also discussed. On the other hand, solution-processed graphene combines the unique optoelectrical properties of graphene with large area deposition and flexible substrates making it compatible with printing and coating technologies, such as roll-to-roll, inkjet, gravure, and flexographic printing manufacturing methods. This chapter provides an overview of the most recent research progress in the application of solution-processed graphene-based films as transparent conductive electrodes (TCEs) in OSCs. (a) Chemically converted graphene (CCG), (b) thermally and photochemically reduced graphene oxide, (c) composite reduced graphene oxide-carbon nanotubes, and (d) reduced graphene oxide mesh films have demonstrated their applicability in OSCs as transparent, conductive electrodes.

Keywords: organic solar cells, transparent electrodes, graphene, reduction

1. Introduction

Organic solar cells (OSCs) based on two-dimensional (2D) nanomaterials, including graphene, transition metal dichalcogenides (TMDs), and Xenes (silicene, germanene, stanene, etc.) have experienced immense interest as possible candidates for clean energy generation offer the benefit of low-cost, light-weight, large-area, high mechanical flexibility, and low temperature/high throughput manufacturing processes [1–3] offering important advantages over silicon technology. A key task toward the implementation of this technology is the adaptability and/or the development of the materials used for their fabrication to further optimize their overall performance [4–12].

Transparent conductive electrodes (TCEs) with an outstanding combination of high electrical conductivity and good optical transparency have a crucial role in OSCs, as the first layer of the device that the incident solar electromagnetic radiation should transmit in order to be absorbed by the solar cell's active medium [13–15]. Conventionally, the most common materials are indium tin oxide (ITO) and fluorine tin oxide (FTO), which are widely used as the transparent electrode in many optoelectronic devices because of their good combination of high transparency and low resistance [16–18]. However, these metal oxides exhibit several issues due to the high cost, resulting mostly from the indium scarcity [19], their brittleness [20], the device degradation due to indium diffusion into the photoactive layer [21], and the requirement for high cost coating methods [20]. Significant effort toward the search of alternatives has therefore been motivated [15, 22–24] and several alternative materials have been proposed, including metallic nanowires (NWs), nanostructured carbon, and conductive polymers, among others [24, 25]. Therefore, developing new materials combining most desirable properties for transparent electrodes will contribute to satisfy the increasing demand for low-cost solution-processed flexible devices. Due to its exceptional properties, graphene is highly attractive and is believed to be the next wonder material for optoelectronics; thus, triggering its application as a transparent electrode for flexible energy-harvesting devices [26].

Graphene, a two-dimensional single-atom-thick (0.34 nm) carbon honeycomb, corresponds to the interlayer spacing of graphite [27]. It displays unique thermal conductivity (≈5.0 × 103 W mK^{-1}) [28], superior mechanical strength (remarkable flexibility elastic modulus ~1 TPa), and outstanding chemical stability, especially high electron mobility (>15,000 cm^2 Vs^{-1}) [29], which overcomes the intrinsic performance limitations of traditional transparent electrode materials, as well as low sheet resistance (35 Ω sq^{-1} at 90% optical transmittance) [30], high optical transmittance (≈97.7% for single-layer graphene) [31], and good piezoresistive sensitivity [32].

Graphene production includes several methods. Depending on its quality, the properties of the synthesized graphene may differ. More specifically, the grain size, the shape, the thickness as well as the presence of defects influence graphene mechanical properties. From a highly ordered pyrolytic graphite (HOPG) through a mechanical exfoliation method ("scotch-tape"), originally graphene was produced [33]. Since then, the number of methods for graphene production has significantly increased. Some of them include liquid phase exfoliation (LPE) [34], chemical vapor deposition (CVD) [35], preparation from organic materials using solvothermal method [36], chemical cross-linking of polycyclic aromatic hydrocarbons [37], preparation

http://dx.doi.org/10.5772/67919

from SiC through thermal decomposition [38], and carbon nanotube unzipping [39]. Although CVD method produces the less defective graphene films, it exhibits technical issues relating with the deposition of graphene films on flexible substrates making this method incompatible with roll-to-roll (R2R) mass production processes. On the contrary, the fact that graphene oxide (GO) can be produced in large quantities from low-cost graphite powder and its property to give stable dispersions in various solvents, make GO an ideal candidate for solution-processed graphene production [40]. On top of that, it can be the precursor for conductive inks production, adding to the printing electronics technology [27]. However, the introduction of oxygen functional groups on the GO lattice, disrupts the sp^2 conjugation system of the hexagonal graphene lattice, making GO an insulator. By removing the oxygen containing groups, GO can be partially reduced to conductive graphene-like sheets. The reduction process can be performed by chemical [41], thermal [42], or photochemical treatment [43], aiming to yield reduced graphene oxide (rGO) with similar properties to graphene [41].

This chapter covers the latest advances in solution-processed graphene-based thin films as the anode TCE in OSCs, substituting the conventional ITO. We highlight the latest advances on thermally, chemically and photochemically produced conductive graphene-based nanomaterials, as well as on graphene-based nanocomposites TCE films. In addition, we summarize some promising routes for the graphene-based TCEs treatment that advance their optoelectrical properties tailoring and achieve a balance between the sheet resistance (R_s) and transmittance of the solution-processed graphene-based TCEs. ITO replacement in graphene-based TCEs, establishes the era of lightweight, low cost, extended lifetime, and stability, as well as flexible and stretchable OSCs.

2. Applications of graphene-based TCE in OSCs

Numerous studies have aimed to investigate the key role of graphene-based materials as the anode (positive electrode) in OSCs. A TCE with efficient carrier transport and thus, high charge collection efficiency is required in OSC devices as outlined in **Figure 1**. Properties including high transparency (>80%), low sheet resistance (R_s < 100/sq), suitable work function (4.5–5.2 eV) as well as low cost and compatibility with R2R fabrication processes characterize the ideal TCE material. Despite the unique optoelectrical properties (T > 90%, R_s = 10–20 Ω/sq) of ITO and its ideal work function, the abovementioned ITO disadvantages have intensified the research on graphene-based TCEs in OSCs. In this context, solution-processed graphene-based films meeting the standards for low electrical resistance, high optical transparency and tunable WF must be developed.

2.1. Chemically treated rGO transparent conductive electrodes

In 2008, Wu et al. compared the electrical properties of rGO films prepared according to two different reduction methods: chemical and thermal treatment [44]. As pristine material, graphene oxide (GO) prepared by Hummers' method was used. The conductivity properties of GO reduced by vacuum annealing at 1100°C, by a combination of hydrazine (N_2H_4) treatment,

Figure 1. The graphene-based TCE as the anode in a typical flexible OSC.

and Ar annealing at 400°C were explored. The results displayed that the vacuum annealing reduction resulted in rGO films with slightly better transparency and conductivity compared to the films reduced using the chemical and thermal treatment combination. In both cases, the film surfaces were free from spikes that can cause short circuit in optoelectronic devices. This is an advantage of graphene-based electrodes over carbon nanotube or metal nanowire mesh electrodes, which require a thick, spin-coated polymer buffer layer in order to prevent shorts, generated by rough surfaces (spikes). The transmittance and R_s with respect to the rGO film thickness with the two different fabrication methods are depicted in **Figure 2**. In a general term, for <20 nm film thickness, the optical transmittance was 480%, while the R_s varied from 5 to 1 MΩ sq^{-1}. Bilayer small molecule OSCs were fabricated on rGO/quartz and on ITO/glass substrates. The fabricated cells of the structure rGO/copper phthalocyanine (CuPc)/fullerene (C_{60})/bathocuproine (BCP)/Ag achieved a power conversion efficiency (PCE) of ~0.4%, whereas the ITO-based devices exhibited a PCE of ~0.84%. The observed PCE difference is attributed to the higher R_s of graphene-based electrodes compared to the ITO electrodes.

Yun et al. investigated the potential use of a solution-processed rGO thin film as transparent electrodes and characterized the effect of rGO films by tuning the film thickness and annealing treatment on the cell performances in OSCs [45]. Using a p-toluenesulfonyl hydrazide (p-TosNHNH$_2$) reducing agent, GO reduction took place. rGO dispersions with high concentrations and thin film processability were prepared as a result of the hydrazone groups attached to the edge and basal plane of graphene. In this way, issues created using other film preparation techniques (i.e., transfer problems during vacuum filtration) or high temperature reduction methods could be overwhelmed [46, 47]. They also evaluated the morphological and optical properties of the solution-processed rGO thin films by tuning the fabrication conditions, such

http://dx.doi.org/10.5772/67919

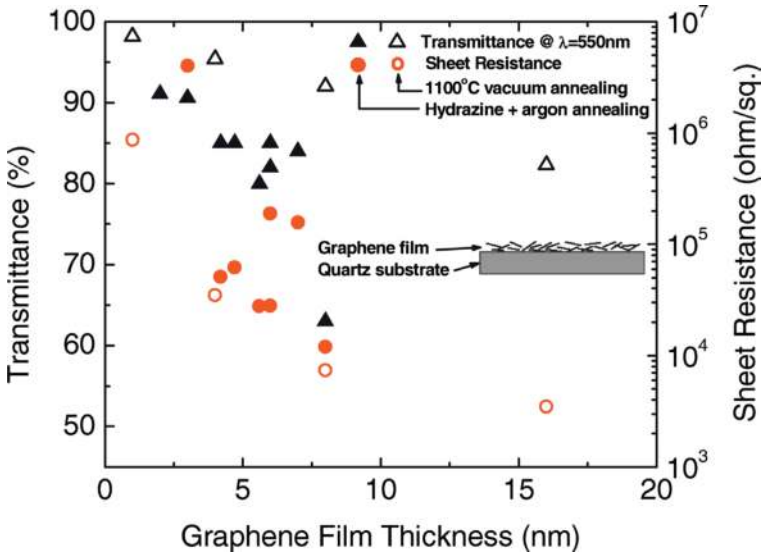

Figure 2. Transmittance at $\lambda = 550$ nm (triangles) and sheet resistance (circles) as a function of the graphene film thickness for both reduction methods: vacuum annealing at 1100°C (open symbols) and hydrazine treatment and Ar annealing at 400°C (filled symbols). Reprinted with permission from Wu et al. [44]. Copyright 2008 AIP Publishing LLC.

as spin-coating cycles and annealing temperatures. All rGO thin films fabricated through a spinning method showed a highly uniform morphology with thickness controllability. In addition, sheet resistance was efficiently decreased from ~103 to 10 kΩ sq^{-1} by the trade-off between the coating cycles and the annealing conditions. Finally, the effects of rGO-based electrodes on the OSC performances by controlling the number of coating cycles were studied. OSCs performance was improved upon decreasing the sheet resistance, for 200°C as the annealing temperature and seven times coated rGO film, achieving a PCE of 0.33%.

In 2015, Moaven et al. reported the synthesis of an rGO/Ag nanocomposite electrode appropriate for OSCs [48]. The reported technique is applicable to flexible substrates by spin coating of an aqueous solution of rGO/Ag nanocomposite on polyethylene terephthalate (PET) substrate in ambient conditions. The optical and electrical properties were determined by tuning the Ag concentration of the rGO/Ag nanocomposite and the electrode thickness. Flexible electrodes were prepared with R_s as low as 83 kΩ sq^{-1} and with a transmittance of 47%. Finally, OSCs onto PET, based on rGO/Ag anode electrode in different ratios were fabricated. The highest PCE observed was 0.24% onto PET flexible substrates which was improved by 25% compared to the conventional ITO/glass (0.18%).

Huang et al. in another article, demonstrated the preparation of highly conductive and transparent graphene-based electrodes with tunable WFs by mixing single walled carbon nanotubes (SWCNTs) with chemically reduced GO [49]. More specifically, dry powders of GO and SWCNTs were directly dispersed in anhydrous hydrazine. The yielded composite was coated in different thicknesses (1–5 layers) and the optical and electrical properties of the fabricated

films were characterized. The transmittance was directly affected by the number of spin-cast layers, as presented in **Figure 3**. By increasing the number of spin-cast layers from one to five, the optical transmittance at 550 nm was decreased from 88.8 to 58.7%. On the other hand, sheet resistance values of the rGO-SWCNT films were conversely affected upon the increase of the number of spin-cast layers reaching R_s values as low as 254 Ω sq^{-1}. Furthermore, OSCs were fabricated using rGO-SWCNT films as the anode TCE. Through doping with alkali carbonates (Li, Na, Cs, etc.), it is possible to tune the WF of the solution-processed rGO-SWCNTs to match the lowest unoccupied molecular orbital (LUMO) of $PC_{61}BM$. In this way, an improved ohmic contact with the active layer can be achieved, leading to increased charge injection and better device performance. On top of that, SWCNTs can act as conductive percolation paths that short circuit the rGO sheets. Inverted OSCs with structure of rGO-SWCNT/PEDOT:PSS/P3HT:$PC_{61}BM$/V_2O_5/Al were fabricated to demonstrate the applicability of WF tuning of rGO-SWCNT. The devices based on P3HT:$PC_{61}BM$, incorporating the four-layer rGO-SWCNT film exhibited a maximum PCE of 1.27%. Additionally, an excellent flexibility even under bending angles of more than 60° was observed.

2.2. Thermally annealing rGO transparent conductive electrodes

The first application of solution-processed thermally reduced GO TCEs in OSC devices was performed by Yin et al. in 2010 [50]. In more detail, GO films were firstly spin-coated on SiO_2/Si substrates, followed by reduction through thermal annealing at 1000°C in the presence of Ar/H^2. Polymethylmethacrylate (PMMA) (~300 nm thick) was subsequently coated to be used as an intermediate transfer substrate before the final transfer of rGO films onto polyethylene terephthalate (PET) substrates. Flexible poly(3-hexylthiophene) (P3HT):phenyl-C_{61}-butyric acid

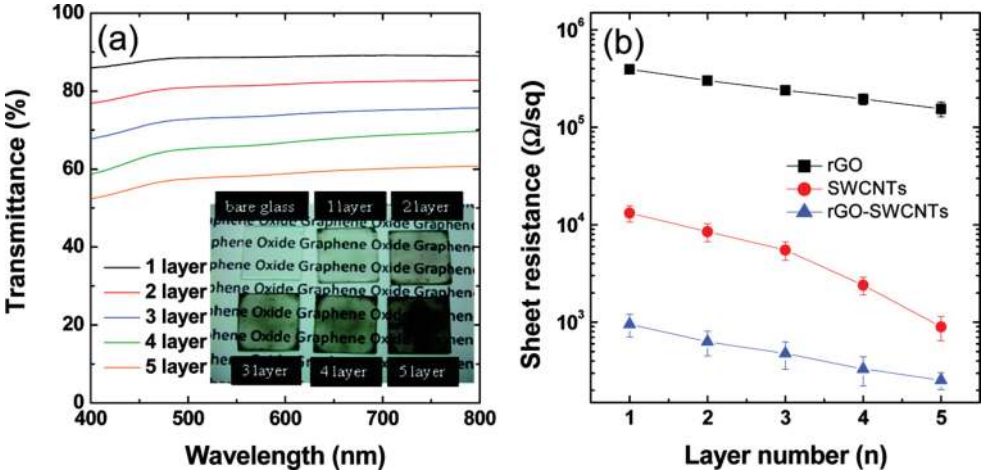

Figure 3. (a) rGO-SWCNT films transmission spectra featuring different numbers of deposited layers. Inset: photograph of the samples tested. (b) rGO, SWCNTs, and the hybrid rGO-SWCNT sheet resistances as a function of the layers' number. A significant decrease of the rGO sheet resistance is demonstrated after adhering to the SWCNTs. Reprinted with permission from Huang et al. [49]. Copyright 2011 ACS American Chemical Society.

http://dx.doi.org/10.5772/67919

methyl ester ($PC_{61}BM$)–based OSCs were fabricated on the rGO-coated PET substrates, and the electrical characteristics of the OSCs were investigated with respect to the thickness of the rGO electrode (**Figure 4**).

Higher device performance dependence on the rGO film R_s was observed when the rGO films optical transmittance exceeded 65%, while the light transmission efficiency dominated the OSCs performance in lower optical transmittance (<65%). The optimum power conversion efficiency (PCE) was achieved for device 3 (PCE = 0.78%), slightly lower than the one reported for CVD-graphene/PET-based photovoltaic devices (1.18%) [15]. This results from the lower R_s of the CVD grown graphene compared to the thermally derived rGO film.

rGO films were also investigated regarding their flexibility as displayed in **Figure 5**. BHJ OSC electrical properties incorporating rGO films as electrodes demonstrated excellent tolerance under high bending conditions and multiple number of bending cycles. The critical point beyond which the fabricated OSCs with rGO/PET films exhibited degradation due to bending depends on the rGO film thickness. In more detail, thicker rGO electrodes led to higher stability, when the OSCs were subjected to tensile stress. After various bending cycles, an electrical degradation of rGO-based OSCs was observed, which was analogous to the increased R_s of the rGO/PET films. In particular, after 1600 bending cycles, the R_s of the rGO/PET electrode increased from 16 to 18 kΩ sq^{-1} and 3.2 to 3.5 kΩ sq^{-1}, respectively, for the 4 and 16 nm thick rGO films.

In another study, Geng et al. reported a simple method for preparing graphene TCEs using seriatim a chemical and a thermal reduction method [51]. More specifically, a converted graphene (CCG) suspension obtained via controlled chemical reduction of exfoliated GO in the absence of dispersants was used as the pristine material and then, upon thermal annealing for 15 min at three different temperatures (200, 400, and 800°C) under vacuum in a furnace tube, the sp^2 carbon networks of the graphene sheets were recovered, with the resulting CCG

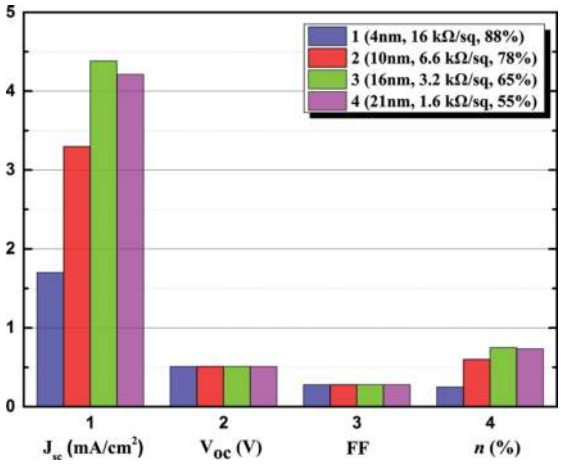

Figure 4. The effect of the rGO transparent films thickness in the performance of P3HT:$PC_{61}BM$ BHJ OSCs. Reprinted with permission from Petridis et al. [26]. Reproduced by permission of The Royal Society of Chemistry.

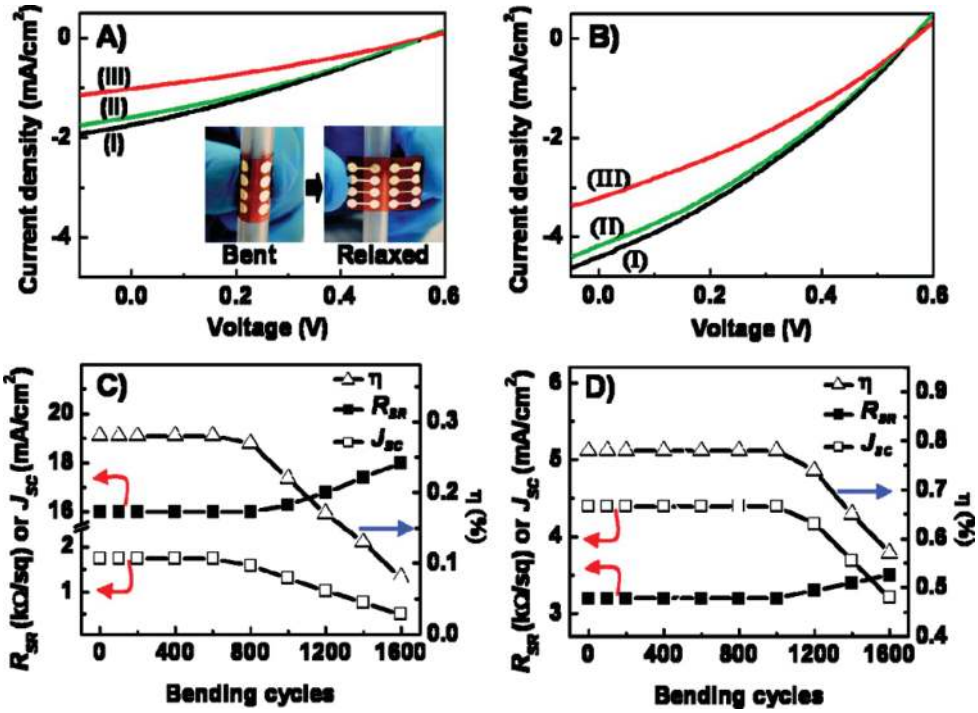

Figure 5. Current density-voltage (*J-V*) curves the various devices tested: (A) for device 1 after applying (i) 400, (ii) 800, and (iii) 1200 cycles of bending, and (B) for device 3 after (I) 800, (II) 1200, and (III) 1600 cycles of bending. (C) and (D) The short circuit current density, overall power conversion efficiency (n), and sheet resistance R_{SR} for devices 1 and 3, respectively, as a function of the number of bending cycles. Reprinted with permission from Yin et al. [50]. Copyright 2010 ACS American Chemical Society.

films exhibiting an R_s of the order of 103 Ω sq^{-1} at 50% transparency (at 550 nm). Owing to the apparently greater extent of sp^2 carbon networks restoration during the two-step reduction of the CCG films, each thermally annealed CCG film exhibited lower R_s than the thermally annealed GO as depicted in **Figure 6**. The transparency of the CCG films decreases linearly with respect to the volume of the CCG suspension used to prepare the vacuum-filtered film, as also displayed in **Figure 6**. By increasing the annealing temperature, the transparency of the CCG films decreased due to thermal improvement of the sp^2 carbon networks in the CCG sheets.

The recession of the R_s observed in **Figure 6**, as the annealing temperature increases, is attributed to the smaller induced distance owing to the elimination of the functional groups between the CCG sheets layers, which leads to facilitated charge carrier transfer across the CCG sheets. It is observed that interlayer distance in CCG-A800 films is reduced to 0.354 nm, approaching the value of bulk graphite. The transparency reduced from this point, while the R_s was reduced linearly to the order of 10^3 Ω sq^{-1}, demonstrating that reduction impacted successfully and uniformly from the outermost to the inner layers [51].

http://dx.doi.org/10.5772/67919

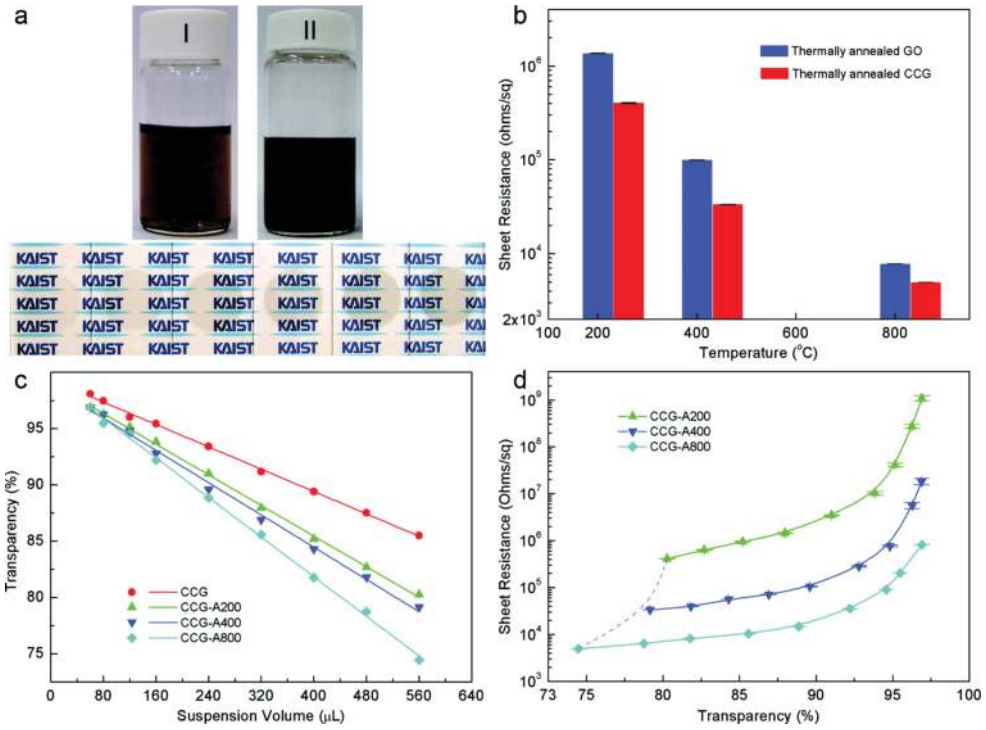

Figure 6. (a) A GO suspension with concentration of 0.1 mg/mL (I), the resultant CCG suspension (II), and the CCG films produced using 160, 240, 320, 400, 480, and 560 μL of a 10 mg/L CCG suspension. (b) GO and CCG films R_s annealed at 200, 400, and 800°C. (c) Transparency of CCG, CCG-A200, CCG-A400, CCG-A800 films with respect to the volume (μL) of the 10 mg/L CCG suspension used for film preparation, and (d) R_s values of CCG-A200, CCG-A400, CCG-A800 films as a function of film transparency. Reprinted with permission from Geng et al. [51]. Copyright 2010 ACS American Chemical Society.

An important conductivity improvement was induced due to the structural changes in the CCG resulted from the thermal reduction. In particular, sp^2 carbon network recover was crucial for increasing the charge carrier transport in individual CCG layers, while the interlayer distance was decreased to a level close to the value of bulk graphite; thereby, improving the charge carrier transport across the CCG layers. As a proof of concept, CCG films were used as TCEs in P3HT:PC_{61}BM-based OSCs achieving a maximum PCE of 1.01%, which is ~50% decreased compared to the PCE value in ITO-based devices, as presented in **Figure 7**.

2.3. Photochemically treated rGO transparent conductive electrodes

For the first time, Kymakis et al. presented a facile, laser-assisted technique to prepare transparent and highly conductive graphene-based films on top of flexible substrates, produced by spin-casting [52]. The experimental setup was realized with (1) a Ti:Sapphire pulsed laser source, (2) a 10 mm diameter lens, and (3) a high precision X-Y computer controlled translation stage where the film was placed and translated across the focused laser beam (**Figure 8**).

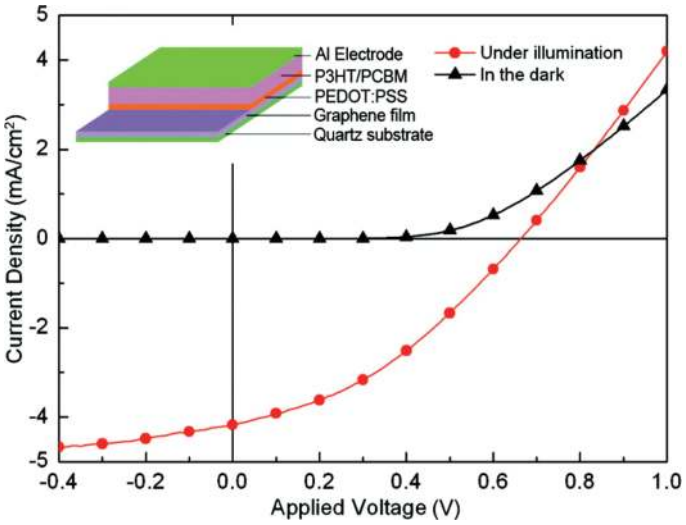

Figure 7. *J-V* curves for P3HT:PC61BM-based OSCs incorporating the CCG-A800 film as TCE. The inset shows the architecture of the solar cell device. Reprinted with permission from Geng et al. [51]. Copyright 2010 ACS American Chemical Society.

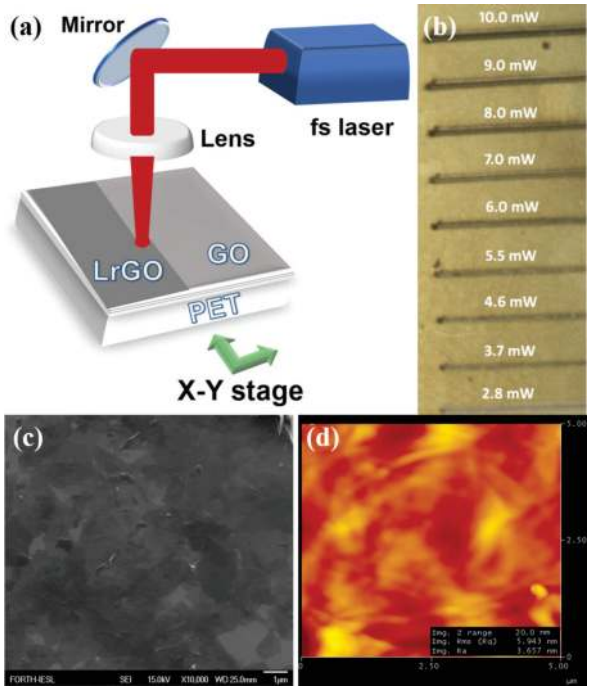

Figure 8. (a) Laser-based GO reduction experimental setup. (b) Scan lines obtained upon irradiation with 100 fs pulses at different fluences indicating the gradual color change due to reduction. (c) SEM and (d) AFM images of LrGO films on PET. Reprinted with permission from Kymakis et al. [52]. Copyright 2013 WILEY-VCH Verlag GmbH & Co. KGaA, Weinheim.

http://dx.doi.org/10.5772/67919

During the reduction process, the fs laser beam irradiated the as-spun GO layers, while it was translated across the layers. The reduction of GO can be obvious. Scan lines obtained upon irradiation with 100 fs pulses at different fluencies indicating the gradual color change due to the reduction are also presented in **Figure 8**. The brownish color of the as cast film was gradually turned into black, which is a strong indication that GO is rapidly reduced via the laser treatment in air, without using any reducing chemical agent. Scanning electron microscopy (SEM) and atomic force microscopy (AFM) analysis demonstrated that no or minor ablation effects occur during the reduction process.

The scope behind the production of solution cast laser reduced GO (LrGO) electrodes is to prepare highly flexible OSCs that can be utilized for compact R2R solar modules. In this context, the LrGO films were used to fabricate flexible OSC devices (**Figure 9**) in order to determine their photovoltaic characteristics and identify the combination of transparency and R_s that provides the best performance. Compared to the thermally reduced GO-based

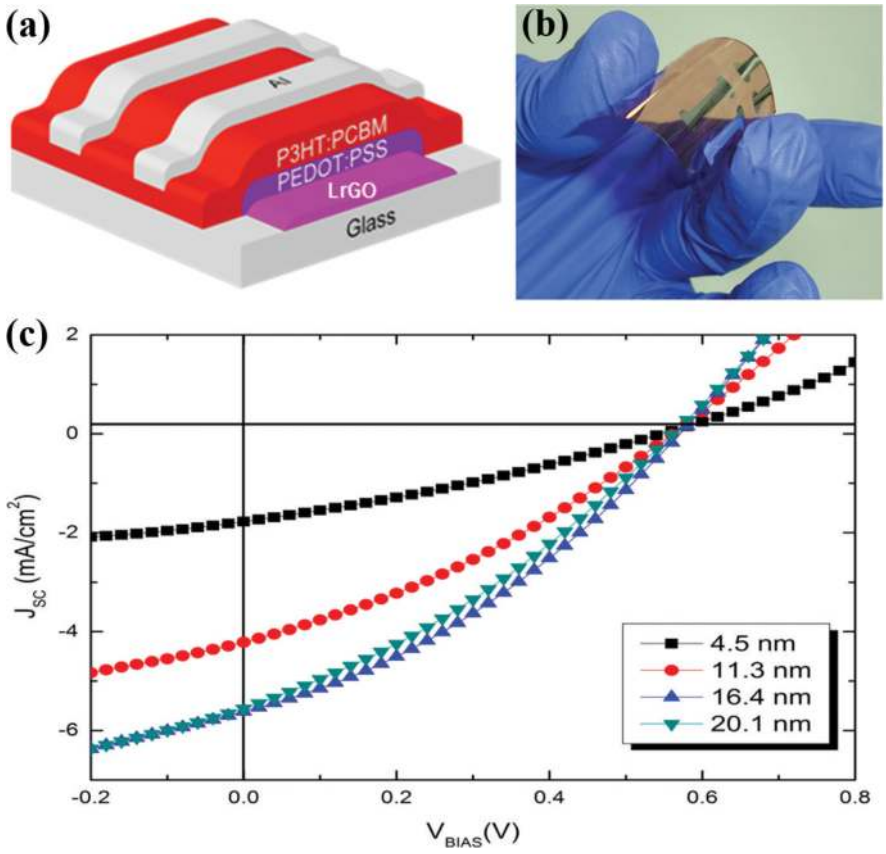

Figure 9. (a) Schematic and (b) picture of the flexible PET/rGO/PEDOT:PSS/P3HT:PC_{61}BM/Al photovoltaic devices fabricated and (c) The illuminated current density-voltage (*J-V*) curves of the solar cells with various LrGO film thicknesses. Reprinted with permission from Kymakis et al. [52]. Copyright 2013 WILEY-VCH Verlag GmbH & Co. KGaA, Weinheim.

OSC devices (PCE ~ 0.78%) [50], LrGO-based OSCs exhibited 41% efficiency improvement for a 16.4 nm thick film having an R_s of 1.6 kΩ sq^{-1} and 70% transparency. It is clear that the higher efficiency is attributed to the LrGO film, revealing the superiority of the laser ablation method, in contrast to the chemical method.

Since rGO TCEs presents low performance in terms of conductivity and transmittance (R_s ~1 kΩ sq^{-1}, 70% transmittance) compared to the ITO TCEs (R_s ~15 Ω sq^{-1}, 90% transmittance), new efforts are performed to improve graphene-based TCE performances. One very promising technique is the employment of a mesh structure with periodic lines on the rGO film [53], with OSC devices based on graphene mesh electrodes (GMEs) already exhibiting performances comparable to those using conventional ITO TCEs [54, 55]. Therefore, it is possible to control the films R_s and transparency by tailoring the grid width, spacing, and thickness [56].

In the same year, Zhang et al. demonstrated the preparation of graphene mesh electrodes (GMEs) by using the standard industrial photolithography and O_2 plasma etching process as illustrated in **Figure 10** [57]. The R_s and the transparency of the graphene TCEs before the mask-based etching were 150 Ω sq^{-1} and ~8%, while after the etching technique, the electrodes R_s and transparency were measured to be 750 Ω sq^{-1} and 65%, respectively. The GME transparency was directly designated by (a) pit depth and (b) period of the mesh, while its conductance was mainly affected by the mesh (a) pit depth and (b) linewidth. By adjusting the duration of the O_2 process, the pit depth was controlled, with 4–10 min of O_2 plasma etching time required for high transparent mesh pits. To further investigate the appropriateness of the GMEs, OSC devices of the structure GME/PEDOT:PSS/P3HT:PC_{61}BM/LiF/Al were fabricated. The devices employing optimum pit depth GMEs exhibited a PCE equal to 2.04% decreased by ~33% compared to the conventional ITO-based OSCs (PCE ~3%).

In 2015, Konios et al. presented a different laser-assisted method to directly pattern a mesh on the surface of rGO films deposited onto flexible substrates, for the production of large area reduced graphene oxide micromesh (rGOMM) electrodes [58]. By using this technique, the use of complicated photolithographic [59], ion beam [60], chemical etching [61], template [62] and O_2 plasma methods [52] was overtaken. The proposed technique is a one-step method,

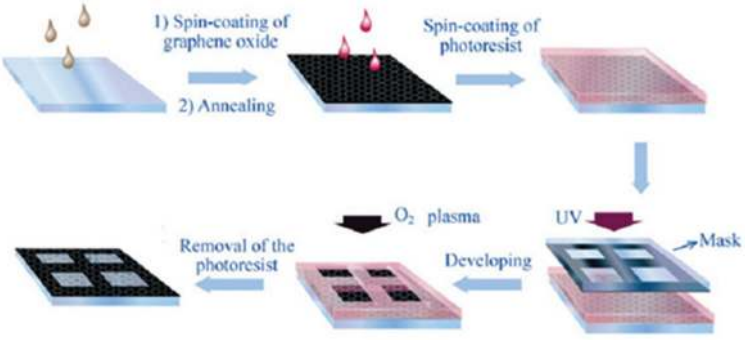

Figure 10. Illustration of the fabrication steps for the preparation of GMEs. Reprinted with permission from Zhang et al. [57]. Copyright 2013 Springer Berlin Heidelberg.

http://dx.doi.org/10.5772/67919

since no TEM grid patterning mask [63], and no transfer step are needed. In addition, the method does not use any photo-resistive material [64] or pre-patterned elastomeric stamps [65], while the application of a fs laser pulses allows the patterning of micro size holes on top of any flexible low cost material. In addition, this technique can be easily controlled over the entire illuminated area induces minimum thermal damage in the surrounding layers and more importantly is compatible to R2R production processes.

The electrode transparency can be accurately controlled with a small R_s increase, successfully handling with the existing trade-off between transparency and electrical conductivity. The rGO thin films optoelectrical properties of depended on the interplay between the periodicity and the geometrical characteristics of the mesh pattern structure. The rGO mesh electrode experimental setup and SEM images of the laser-induced patterns are presented in **Figure 11**. The proposed technique main advantage is that it permits fine-tuning of the optoelectrical properties via variation of the irradiation dose (energy, number of pulses) and/or the periodicity and thus the neck width of the mesh. A significant improvement of the transmittance by ~65% was performed after laser treatment. As a proof of concept, reduced GO micromesh (rGOMM) were employed as the anode TCE in flexible devices based on poly[N-90-heptadecanyl-2,7-carbazole-alt-5,5-(40,70-di-2-thienyl20,10,30-benzothiadiazo-le)] (PCDTBT):[6, 6]-phenyl C71 butyric acid methyl ester ($PC_{71}BM$) and compared with those deposited on ITO (**Figure 12**).

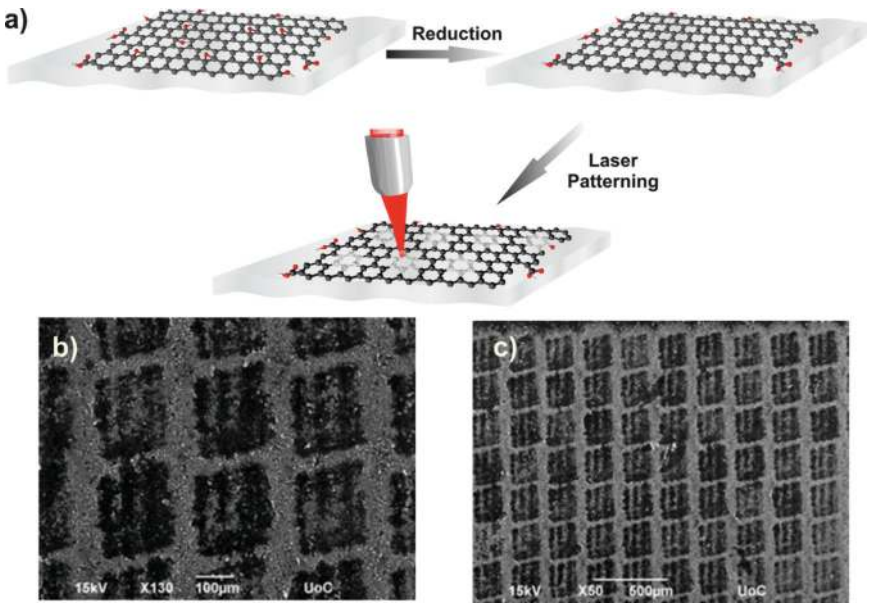

Figure 11. (a) Illustration of the laser-induced patterns on the rGO films and (b, c) SEM images of the laser-induced patterns: the darker spots correspond to the laser-processed areas where the mesh lines correspond to the lighter colored paths. Reprinted with permission from Konios et al. [58]. Copyright 2015 WILEY-VCH Verlag GmbH & Co. KGaA, Weinheim.

The optimum photovoltaic parameters for the rGOMM-based devices were extracted for transparency ~59.1% and R_s ~565 Ω sq^{-1}, with the resulting PCE of 3.05%, the highest reported so far for flexible OSC devices incorporating solution-processed graphene-based electrodes. Another important issue investigated in this study was the determination of the effectiveness of the proposed method when tested in large area photovoltaic cells, as presented in **Figure 12**. This is very important for upscaling from lab solar cells to solar modules. In this context, stress tests demonstrated that the photovoltaic performance deterioration for both rGOMM and ITO electrodes tested was almost the same; for 135 mm^2 active area PCE reduction measured was 63.2% for ITO and 64.9% for rGOMM, respectively. Therefore, the proposed method can be effectively applied when upscaling to large area photovoltaic cells or solar modules without compromising the photovoltaic efficiency compared with the widely commercialized ITO transparent electrode.

During the last 5 years, an intensive research effort was conducted in the field of solution-processed graphene-based TCEs (**Figure 13**). The optoelectrical properties of graphene-based TCEs in OSCs are presented in **Table 1**. The increase of the PCE of OSC devices incorporating graphene-based TCEs has been improved from 0.13 to 3.7% for rigid devices, while the progress on the flexible graphene-based devices was also incredible with an efficiency improvement from 0.78 to 3.05%.

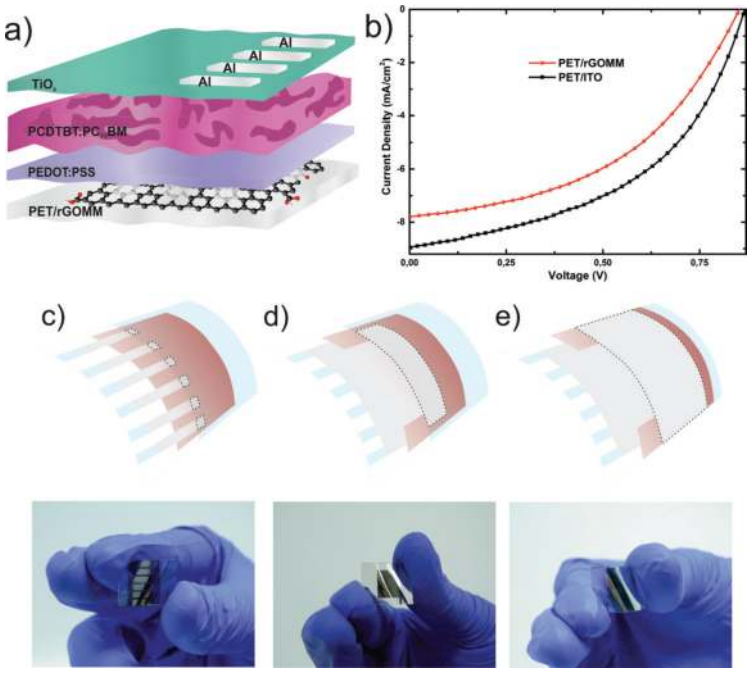

Figure 12. (a) The architecture of the BHJ OSC device with the laser-induced rGOMM as TCE. (b) Photovoltaic performance of the OSCs with rGOMM (spheres) and ITO (squares) as TCE. Schematic illustration and photographs of (c) 4 mm^2, (d) 50 mm^2 and (e) 135 mm^2 active areas devices tested. Reprinted with permission from Konios et al. [58]. Copyright 2015 WILEY-VCH Verlag GmbH & Co. KGaA, Weinheim.

http://dx.doi.org/10.5772/67919

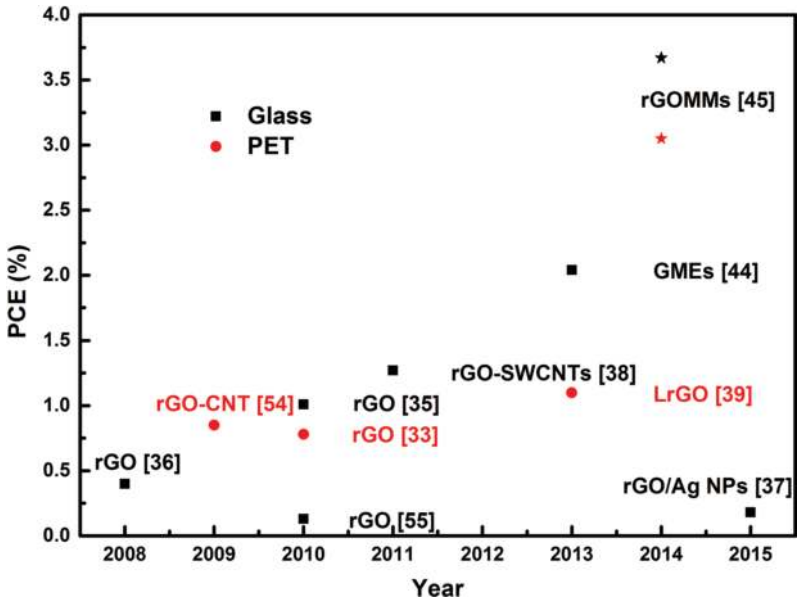

Figure 13. OSCs performance of solution-processed graphene-based TCE with different active layers extracted from literature [44, 48–51, 57, 58, 66, 67]. Squares stand for rigid devices, whereas circles for devices on flexible substrates. Stars illustrate the champion PCE achieved. Reprinted with permission from Konios et al. [58]. Copyright 2015 WILEY-VCH Verlag GmbH & Co. KGaA, Weinheim.

Graphene-based electrodes	R_s (kΩ/sq)	Transparency (%)	Reference
Thermal reduced GO	3.2	65	[50]
Thermal reduced GO	1	80	[51]
LrGO	1.6	70	[52]
rGO-SWCNTs	0.331	65.8	[49]
rGO mesh electrodes	0.700	65	[57]
LrGO mesh electrode	0.565	59.1	[58]
rGO/Ag NPs	83	47	[48]

Reprinted with permission from Petridis et al. [26]. Reproduced by permission of The Royal Society of Chemistry.

Table 1. Summary of the optoelectrical properties of graphene-based TCEs in OSC devices.

3. Conclusion

In this chapter, the concept of solution-processed graphene-based films as anode electrodes in OSCs has been presented, with respect to the fabrication techniques used: (a) thermally reduced graphene, (b) chemically and photochemically rGO, (c) composite rGO-CNTs, and (d) rGO mesh

films. The application of rGO-based TCEs in OSCs was also demonstrated. The successful transferring of such schemes in large scale poses a significant engineering challenge and ongoing effort is needed for preparing high efficient printed optoelectronic devices such as flexible and stretchable OSCs. Despite graphene-based materials advantages regarding the manufacturing and purchase cost, compatibility with flexible materials, WF tuning (by controlling graphene size, layer and through functionalization), transparency, and solubility, significant improvement is required in order to overcome the corresponding properties of ITO films. Even though the current performance of graphene-based TCE OSCs approaches that of the conventional ITO technology, there is more space for the improvement of OSCs adapting graphene as an anode electrode.

Future research efforts should be focused on (a) inventing cost-effective techniques for large-scale graphene or rGO production, (b) effectiveness improvement of the GO reduction methods, (c) enhancing the electrical conductivity of the graphene-based TCEs without disrupting their transmittance, and (d) improving the graphene-based films morphology. For improving the TCE conductivity, metal nanoparticles (e.g., Au, Ag, and Al) with different sizes and shapes can be incorporated in the graphene-based electrodes, leading to the production of graphene-NPs electrodes with even lower resistance and high mechanical stability; and thus, may improve the overall stability of the devices, contributing to the lifetime enhancement. On top of that, hybrid films consisting of rGO and 1D conductive bridging materials, such as metal nanowires, which exhibit better mechanical properties than ITO films, can significantly decrease the film resistance. The metal nanowires can provide electric pathways among the graphene layers and thus may enhance the conductivity, without sacrificing their optical properties, leading to improved performance of graphene-based TCEs. The incorporation of metal-graphene–based TCEs into optoelectronic devices demonstrates their potential for ITO replacement in a broad range of optoelectronic applications.

Acknowledgements

We acknowledge funding from the European Union's Horizon 2020 research and innovation programme under grant agreement No. 696656 – GrapheneCore1.

Author details

Minas M. Stylianakis[1]*, Dimitrios Konios[1], Konstantinos Petridis[1,2] and Emmanuel Kymakis[1]

*Address all correspondence to: stylianakis@staff.teicrete.gr

1 Department of Electrical Engineering, Center of Materials Technology and Photonics, School of Applied Technology, University of Applied Sciences of Crete (Technological Educational Institute (TEI) of Crete), Heraklion, Crete, Greece

2 Department of Electronic Engineering, University of Applied Sciences of Crete (Technological Educational Institute (TEI) of Crete), Chania, Crete, Greece

References

[1] Bonaccorso F, Colombo L, Yu G, Stoller M, Tozzini V, Ferrari AC, Ruoff RS, Pellegrini V. Graphene, related two-dimensional crystals, and hybrid systems for energy conversion and storage. Science. 2015;**347**:6217. DOI: 10.1126/science.1246501

[2] Chang DW, Choi HJ, Filer A, Baek JB. Graphene in photovoltaic applications: Organic photovoltaic cells (OPVs) and dye-sensitized solar cells (DSSCs). Journal of Materials Chemistry A. 2014;**2**:12136-12149. DOI: 10.1039/C4TA01047G

[3] Chowdhury TH, Islam A, Mahmud Hasan AK, Terdi MAM, Arunakumari M, Prakash Singh S, Alam MDK, Bedja IM, Hafidz Ruslan M, Sopian K, Amin N, Akhtaruzzaman MD. Prospects of graphene as a potential carrier-transport material in third-generation solar cells. The Chemical Record. 2016;**16**:614-632. DOI: 10.1002/tcr.201500206

[4] Balis N, Stratakis E, Kymakis E. Graphene and transition metal dichalcogenide nanosheets as charge transport layers for solution processed solar cells. Materials Today. 2016;**19**:580-594. DOI: 10.1016/j.mattod.2016.03.018

[5] Stylianakis MM, Sygletou M, Savva K, Kakavelakis G, Kymakis E, Stratakis E. Photochemical synthesis of solution-processable graphene derivatives with tunable bandgaps for organic solar cells. Advanced Optical Materials. 2015;**5**:658-666. DOI: 10.1002/adom.201400450

[6] Bonaccorso F, Balis N, Stylianakis MM, Savarese M, Adamo C, Gemmi M, Pellegrini V, Stratakis E, Kymakis E. Functionalized graphene as an electron-cascade acceptor for air-processed organic ternary solar cells. Advanced Functional Materials. 2015;**25**:3870-3880. DOI: 10.1002/adfm.201501052

[7] Stylianakis MM, Konios D, Kakavelakis G, Charalambidis G, Stratakis E, Coutsolelos AG, Kymakis E, Anastasiadis SH. Efficient ternary organic photovoltaics incorporating a graphene-based porphyrin molecule as a universal electron cascade material. Nanoscale. 2015;**7**:17827-17835. DOI: 10.1039/C5NR05113D

[8] Stylianakis MM, Mikroyannidis JA, Kymakis E. A facile, covalent modification of single-wall carbon nanotubes by thiophene for use in organic photovoltaic cells. Solar Energy Materials & Solar Cells. 2010;**94**:267-274. DOI: 10.1016/j.solmat.2009.09.013

[9] Stylianakis MM, Spyropoulos GD, Stratakis E, Kymakis E. Solution-processable graphene linked to 3,5-dinitrobenzoyl as an electron acceptor in organic bulk heterojunction photovoltaic devices. Carbon. 2012;**50**:5554-5561. DOI: 10.1016/j.carbon.2012.08.001

[10] Kakavelakis G, Konios D, Stratakis E, Kymakis E. Enhancement of the efficiency and stability of organic photovoltaic devices via the addition of a lithium-neutralized graphene oxide electron-transporting layer. Chemistry of Materials. 2014;**26**:5988-5993. DOI: 10.1021/cm502826f

[11] Stylianakis MM, Stratakis E, Koudoumas E, Kymakis E, Anastasiadis SH. Organic bulk heterojunction photovoltaic devices based on polythiophene-graphene composites. ACS Applied Materials & Interfaces. 2012;**4**:4864-4870. DOI: 10.1021/am301204g

[12] Balis N, Konios D, Stratakis E, Kymakis E. Ternary organic solar cells with reduced graphene oxide-Sb_2S_3 hybrid nanosheets as the cascade material. ChemNanoMat. 2015;**1**:346-352. DOI: 10.1002/cnma.201500044

[13] Hecht DS, Hu L, Irvin G. Emerging transparent electrodes based on thin films of carbon nanotubes, graphene, and metallic nanostructures. Advanced Materials. 2011;**23**:1482-1513. DOI: 10.1002/adma.201003188

[14] Kumar A, Zhou C. The race to replace tin-doped indium oxide: Which material will win?. ACS Nano. 2010;**4**:11-14. DOI: 10.1021/nn901903b

[15] Gomez De Arco L, Zhang Y, Schlenker CW, Ryu K, Thompson ME, Zhou C. Continuous, highly flexible, and transparent graphene films by chemical vapor deposition for organic photovoltaics. ACS Nano. 2010;**4**:2865-2873. DOI: 10.1021/nn901587x

[16] Li G, Shrotriya V, Huang J, Yao Y, Moriarty T, Emery K, Yang Y. High-efficiency solution processable polymer photovoltaic cells by self-organization of polymer blends. Nature Materials. 2005;**4**:864-868. DOI: 10.1038/nmat1500

[17] Kim Y, Cook S, Tuladhar SM, Choulis SA, Nelson J, Durrant JR, Bradley DDC, Giles M, McCulloch I, Ha CS, Ree M. A strong regioregularity effect in self-organizing conjugated polymer films and high-efficiency polythiophene:fullerene solar cells. Nature Materials. 2006;**5**:197-203. DOI: 10.1038/nmat1574

[18] Klaus E. Past achievements and future challenges in the development of optically transparent electrodes. Nature Photonics. 2012;**6**:809-812. DOI: 10.1038/nphoton.2012.282

[19] Cheng YJ, Yang SH, Hsu CS. Synthesis of conjugated polymers for organic solar cell applications. Chemical Reviews. 2009;**109**:5868-5923. DOI: 10.1021/cr900182s

[20] Mishra A, Bäuerle P. Small molecule organic semiconductors on the move: Promises for future solar energy technology. Angewandte Chemie International Edition. 2012;**51**:2020-2067. DOI: 10.1002/anie.201102326

[21] Scharber MC, Sariciftci NS. Efficiency of bulk-heterojunction organic solar cells. Progress in Polymer Science. 2013;**38**:1929-1940. DOI: 10.1016/j.progpolymsci.2013.05.001

[22] Tan YW, Zhang Y, Bolotin K, Zhao Y, Adam S, Hwang EH, Das Sarma S, Stormer HL, Kim P. Measurement of scattering rate and minimum conductivity in graphene. Physical Reviews Letters. 2007;**99**:246803. DOI: 10.1103/PhysRevLett.99.246803

[23] Roy-Mayhew JD, Aksay LA. Graphene materials and their use in dye-sensitized solar cells. Chemical Reviews. 2014;**114**:6323. DOI: 10.1021/cr400412a

[24] Layani M, Kamyshny A, Magdassi S. Transparent conductors composed of nanomaterials. Nanoscale. 2014;**6**:5581-5591. DOI: 10.1039/C4NR00102H

[25] Rana K, Singh J, Ahn JH. A graphene-based transparent electrode for use in flexible opto-electronic devices. Journal of Materials Chemistry C. 2014;**2**:2646-2656. DOI: 10.1039/C3TC32264E

[26] Petridis C, Konios D, Stylianakis MM, Kakavelakis G, Sygletou M, Savva K, Tzourmpakis P, Krassas M, Vaenas N, Stratakis E, Kymakis E. Solution processed reduced graphene oxide electrodes for organic photovoltaics. Nanoscale Horizons. 2016;**1**:375-382, DOI: 10.1039/C5NH00089K

[27] Torrisi F, Hassan T, Wu W, Sun Z, Lombardo A, Kulmala TS, Hsieh G, Jung S, Bonaccorso F, Paul PJ, Chu V, Ferrari AC. Inkjet-printed graphene electronics. ACS Nano. 2012;**6**:2992-3006. DOI: 10.1021/nn2044609

[28] Bae S, Kim H, Lee Y, Xu X, Park JS, Zheng Y, Balakrishnan J, Lei T, Kim HR, Song YI. Roll-to-roll production of 30-inch graphene films for transparent electrodes. Nature Nanotechnology. 2010;**5**:574-578. DOI: 10.1038/nnano.2010.132

[29] Na SI, Kim SS, Jo J, Kim DY. Efficient and flexible ITO-free organic solar cells using highly conductive polymer anodes. Advanced Materials. 2008;**20**:4061-4067. DOI: 10.1002/adma.200800338

[30] Eda G, Chhowalla M. Chemically derived graphene oxide: Towards large-area thin-film electronics and optoelectronics. Advanced Materials. 2010;**22**:2392-2415. DOI: 10.1002/adma.200903689

[31] Nair R, Blake P, Grigorenko A, Novoselov K, Booth T, Stauber T, Peres N, Geim A. Fine structure constant defines visual transparency of graphene. Science. 2008;**320**:1308. DOI: 10.1126/science.1156965

[32] Smith AD, Niklaus F, Paussa A, Vaziri S, Fischer AC, Sterner M, Forsberg F, Delin A, Esseni D, Palestri P, Östling M, Lemme MC. Electromechanical piezoresistive sensing in suspended graphene membranes. Nano Letters. 2013;**13**:3237-3242. DOI: 10.1021/nl401352k

[33] Novoselov KS, Geim AK, Morozov SV, Jiang D, Zhang Y, Dubonos SV, Grigorieva IV, Firsov AA. Electric field effect in atomically thin carbon films. Science. 2004;**306**:666-669. DOI: 10.1126/science.1102896

[34] Behabtu N, Lomeda JR, Green MJ, Higginbotham AL, Sinitskii A, Kosynkin DV, Tsentalovich D, Parra Vasquez ANG, Schmidt J, Kesselman E, Cohen Y, Talmon Y, Tour JM, Pasquali M. Spontaneous high-concentration dispersions and liquid crystals of graphene. Nature Nanotechnology. 2010;**5**:406-411. DOI: 10.1038/nnano.2010.86

[35] Kim KS, Zhao Y, Jang H, Lee SY, Kim JM, Kim KS, Ahn JH, Kim P, Choi JY, Hong BH. Large-scale pattern growth of graphene films for stretchable transparent electrodes. Nature. 2009;**457**:706-710. DOI: 10.1038/nature07719

[36] Choucair M, Thordason P, Stride JA. Gram-scale production of graphene based on solvo-thermal synthesis and sonication. Nature Nanotechnology. 2009;**4**:30-33. DOI: 10.1038/nnano.2008.365

[37] Wang X, Zhi L, Tsao N, Tomovic Z, Li J, Mullen K. Transparent carbon films as electrodes in organic solar cells. Angewandte Chemie International Edition. 2008;**47**:2990-2992. DOI: 10.1002/anie.200704909

[38] Berger C, Song Z, Li T, Orbazghi AY, Feng R, Dai Z, Marchenkov AN, Conrad EH, First PN, De Heer WA, Ultrathin epitaxial graphite: 2D electron gas properties and a route toward graphene-based nanoelectronics. Journal of Physical Chemistry B. 2004;**108**:19912-19916. DOI: 10.1021/jp040650f

[39] Zhuang N, Liu C, Jia L, Wei L, Cai J, Guo Y, Zhang Y, Hu X, Chen J, Chen X, Tang Y. Clean unzipping by steam etching to synthesize graphene nanoribbons. Nanotechnology. 2013:**24**:325604. DOI: 10.1088/0957-4484/24/32/325604

[40] Konios D, Stylianakis MM, Stratakis E, Kymakis E. Dispersion behaviour of graphene oxide and reduced graphene oxide. Journal of Colloid Interface Science. 2014;**430**:108-112. DOI: 10.1016/j.jcis.2014.05.033

[41] Stankovich S, Dikin DA, Piner RD, Kohlhaas KA, Kleinhammes A, Jia Y, Wu Y, Nguyen ST, Ruoff RS. Synthesis of graphene-based nanosheets via chemical reduction of exfoliated graphite oxide. Carbon. 2007;**45**:1558-1565. DOI: 10.1016/j.carbon.2007.02.034

[42] Mattevi C, Eda G, Agnoli S, Miller S, Mkhoyan KA, Celik O, Mastrogiovanni D, Granozzi G, Garfunkel E, Chhowalla M. Evolution of electrical, chemical, and structural properties of transparent and conducting chemically derived graphene thin films. Advanced Functional Materials. 2009;**19**:2577-2583. DOI: 10.1002/adfm.200900166

[43] Gengler RYN, Badali DS, Zhang D, Dimos K, Spyrou K, Gournis D, Miller RJD. Revealing the ultrafast process behind the photoreduction of graphene oxide. Nature Communication. 2013;**4**:2560. DOI: 10.1038/ncomms3560

[44] Wu J, Becerril H, Bao Z, Liu Z, Chen Y, Peumans P. Organic solar cells with solution-processed graphene transparent electrodes. Applied Physics Letters. 2008;**92**:263302. DOI: 10.1063/1.2924771

[45] Yun JM, Jung CH, Noh YJ, Jeon YJ, Kim SS, Kim DY, Na SI. Morphological, optical, and electrical investigations of solution-processed reduced graphene oxide and its application to transparent electrodes in organic solar cells. Journal of Industrial and Engineering Chemistry. 2015;**21**:877-883. DOI: 10.1016/j.jiec.2014.04.026

[46] Eda G, Fanchini G, Chhowalla M. Large-area ultrathin films of reduced graphene oxide as a transparent and flexible electronic material. Nature Nanotechnology. 2008;3:270-274. DOI: 10.1038/nnano.2008.83

[47] Eda G, Lin YY, Miller S, Chen CW, Su WF, Chhowalla M. Field emission from graphene based composite thin films. Applied Physics Letters. 2008;**92**:23305. DOI: 10.1063/1.3028339

[48] Moaven S, Naji L, Taromi FA, Sharif F. Effect of bending deformation on photovoltaic performance of flexible graphene/Ag electrode-based polymer solar cells. RSC Advances. 2015;**5**:30889-30901. DOI: 10.1039/C5RA00057B

[49] Huang JH, Fang JH, Liu CC, Chu CW. Effective work function modulation of graphene/carbon nanotube composite films as transparent cathodes for organic optoelectronics. ACS Nano. 2011;**5**:6262-6271. DOI: 10.1021/nn201253w

[50] Yin Z, Sun S, Salim T, Wu S, Huang X, He Q, Lam YM, Zhang H. Organic photovoltaic devices using highly flexible reduced graphene oxide films as transparent electrodes. ACS Nano. 2010;**4**:5263-5268. DOI: 10.1021/nn1015874

[51] Geng J, Liu L, Yang SB, Youn SC, Kim DW, Lee JS, Choi JK, Jung HT. A simple approach for preparing transparent conductive graphene films using the controlled chemical reduction of exfoliated graphene oxide in an aqueous suspension. Journal of Physical Chemistry C. 2010;**114**:14433-14440. DOI: 10.1021/jp105029m

[52] Kymakis E, Savva K, Stylianakis MM, Fotakis C, Stratakis E. Flexible organic photovoltaic cells with in situ nonthermal photoreduction of spin-coated graphene oxide electrodes. Advanced Functional Materials. 2013;**23**:2742-2749. DOI: 10.1002/adfm.201202713

[53] Wu H, Hu L, Rowell MW, Kong D, Cha JJ, McDonough JR, Zhu J, Yang Y, McGehee MD, Cui Y. Electrospun metal nanofiber webs as high-performance transparent electrode. Nano Letters. 2010;**10**:4242-4248. DOI: 10.1021/nl102725k

[54] Kang MG, Kim MS, Kim J, Guo LJ. Organic solar cells using nanoimprinted transparent metal electrodes. Advanced Materials. 2008;**20**:4408-4413. DOI: 10.1002/adma.200800750

[55] Yang L, Zhang T, Zhou H, Price S, Wiley BJ, You W. Solution-processed flexible polymer solar cells with silver nanowire electrodes. ACS Applied Materials & Interfaces. 2011;**3**:4075-4084. DOI: 10.1021/am2009585

[56] Zou J, Yip HL, Hau SK, Jen AKY, Metal grid/conducting polymer hybrid transparent electrode for inverted polymer solar cells. Applied Physics Letters. 2010;**96**:203301. DOI: 10.1063/1.3394679

[57] Zhang Q, Wan X, Xing F, Huang L, Long G, Yi N, Ni W, Liu Z, Tian J, Chen Y. Solution-processable graphene mesh transparent electrodes for organic solar cells. Nano Research. 2013;**6**:478-484. DOI: 10.1007/s12274-013-0325-7

[58] Konios D, Petridis C, Kakavelakis G, Sygletou M, Savva K, Stratakis E, Kymakis E. Reduced graphene oxide micromesh electrodes for large area, flexible, organic photovoltaic devices. Advanced Functional Materials. 2015;**25**:2213-2221. DOI: 10.1002/adfm.201404046

[59] Bai J, Zhong X, Jiang S, Huang Y, Duan X. Graphene nanomesh. Nature Nanotechnology. 2010;**5**:190-194. DOI: 10.1038/nnano.2010.8

[60] Sosa NE, Liu J, Chen C, Marks TJ, Hersam MC. Nanoscale writing of transparent conducting oxide features with a focused ion beam. Advanced Materials. 2009;**21**:721-725. DOI: 10.1002/adma.200802129

[61] Zhu Y, Murali S, Stoller MD, Ganesh MJ, Cai W, Ferreira PJ, Pirkle A, Wallace RM, Cychosz KA, Thommes M, Su D, Stach EA, Ruoff RS. Carbon-based supercapacitors produced by activation of graphene. Science. 2011;**332**:1537-1541. DOI: 10.1126/science.1200770

[62] Wang ZL, Xu D, Wang HG, Wu Z, Zhang XB. In situ fabrication of porous graphene electrodes for high-performance energy storage. ACS Nano. 2013;**7**:2422-2430. DOI: 10.1021/nn3057388

[63] Oh JS, Kim SH, Hwang T, Kwon HY, Lee TH, Bae AH, Choi HR, Nam JD. Laser-assisted simultaneous patterning and transferring of graphene. Journal of Physical Chemistry C. 2013;**117**:663-668. DOI: 10.1021/jp309382w

[64] Bie YQ, Zhou YB, Liao ZM, Yan K, Liu S, Zhao Q, Kumar S, Wu HC, Duesberg GS, Cross GLW, Xu J, Peng H, Liu Z, Yu DP. Site-specific transfer-printing of individual graphene microscale patterns to arbitrary surfaces. Advanced Materials. 2011;**23**:3938-3943. DOI: 10.1002/adma.201102122

[65] He Q, Sudibya HG, Yin Z, Wu S, Li H, Boey F, Huang W, Chen P, Zhang H. Centimeter-long and large-scale micropatterns of reduced graphene oxide films: Fabrication and sensing applications. ACS Nano. 2010;**4**:3201-3208. DOI: 10.1021/nn100780v

[66] Tung VC, Chen LM, Allen MJ, Wassei JK, Nelson K, Kaner RB, Yang Y. Low-temperature solution processing of graphene-carbon nanotube hybrid materials for high-performance transparent conductors. Nano Letters. 2009;**9**:1949-1955. DOI: 10.1021/nl9001525

[67] Xu Y, Long G, Huang L, Huang Y, Wan X, Ma Y, Chen Y. Polymer photovoltaic devices with transparent graphene electrodes produced by spin-casting. Carbon. 2010;**48**:3308-3311. DOI: 10.1016/j.carbon.2010.05.017